Electronic Supplementary Material (ESI) for Inorganic Chemistry Frontiers.

Ln-MOFs with window-shaped channels based on triazine tricarboxylic acid as a linker: high-efficient capture of cationic dyes and iodine

Yue Zhao[a], Na Zhang[a], Ying Wang[a], Feng Ying Bai[*a], Yong Heng Xing[*a], Li Xian Sun [b]

[a]College of Chemistry and Chemical Engineering, Liaoning Normal University, Huang he Road 850#, Dalian 116029, P.R. China.

[b]Guangxi Key Laboratory of Information Materials, Guilin University of Electronic Technology, Guilin City, 541004, P.R. China

Supporting Information Contents

Materials and methods. Lanthanide nitrate salts were prepared via dissolving lanthanide oxides with 12 M HNO_3 and then evaporating at 100 °C until the crystal film formed. Other chemicals purchased are not further purified or post-treated. The elemental analysis were carried out on a Perkin-Elmer 240C automatic analyzer. Infrared spectra were measured on a Bruker AXS TENSOR-27 in the range of 400-4000 cm^{-1} at room temperature. UV-Vis spectra were recorded on JASCO V-570 spectrometer (200-2500 nm, in form of solid sample). X-ray powder diffraction (XRD) data were collected on a Bruker Advance-D8 with Cu-Kα radiation, in the range $5^o < 2\theta < 50^o$, with a step size of 0.02^o (2θ) and an acquisition time of 2 s per step. Thermogravimetric analysis (TG) was performed on a Perkin Elmer Diamond TG/DTA under the conditions of the N_2 atmosphere in the temperature range from 30°C to 800°C. The scanning electron microscope (SEM) images were acquired using a SU8010 scanning electron microscope (HITACHI, Tokyo, Japan).

Spectra characteristics of pro-ligand H_3TATAB (Fig.S1-S3).

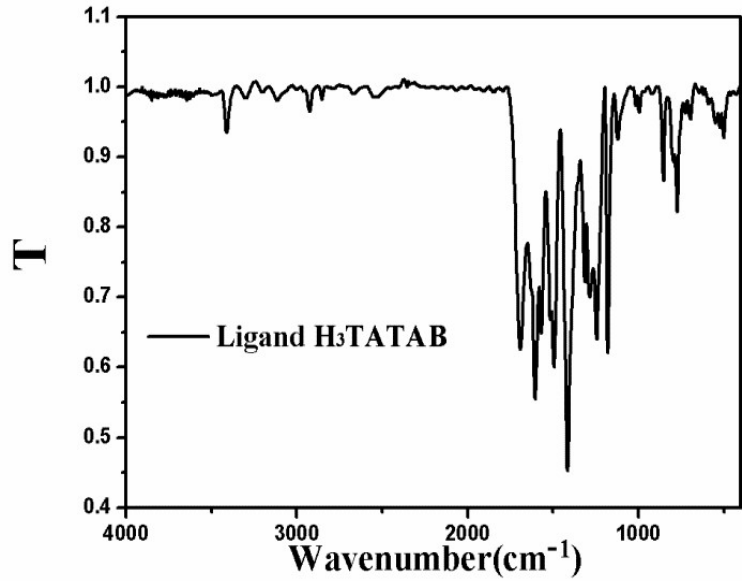

Fig.S1 IR spectrum of pro-ligand H_3TATAB (298K).

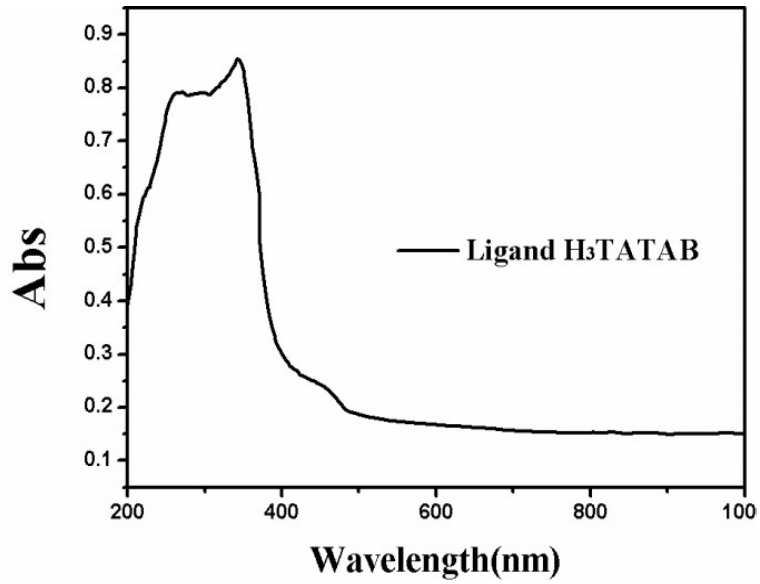

Fig.S2 Solid UV-Vis spectrum of pro-ligand H_3TATAB (298K).

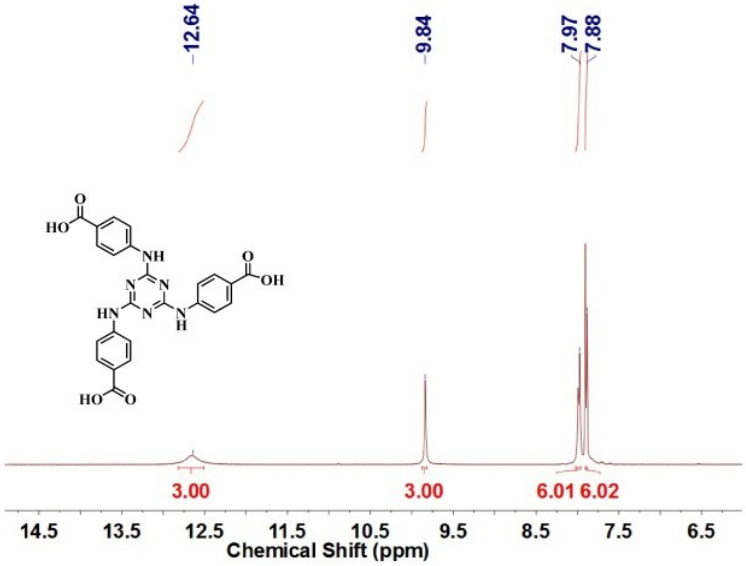

Fig.S3 ^{1}H NMR (400 MHz, d_6-DMSO, 298K) spectrum.

IR spectra of 1-7 at room temperature (Fig.S4-S10).

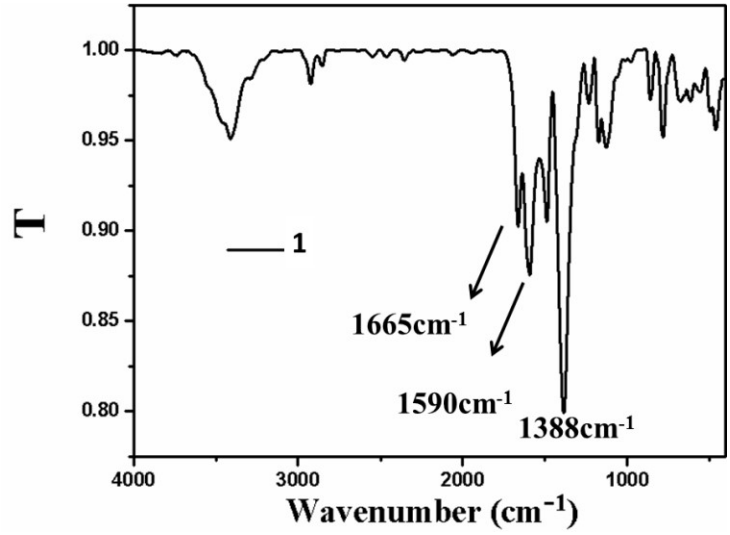

Fig.S4 IR spectrum of **1** at room temperature.

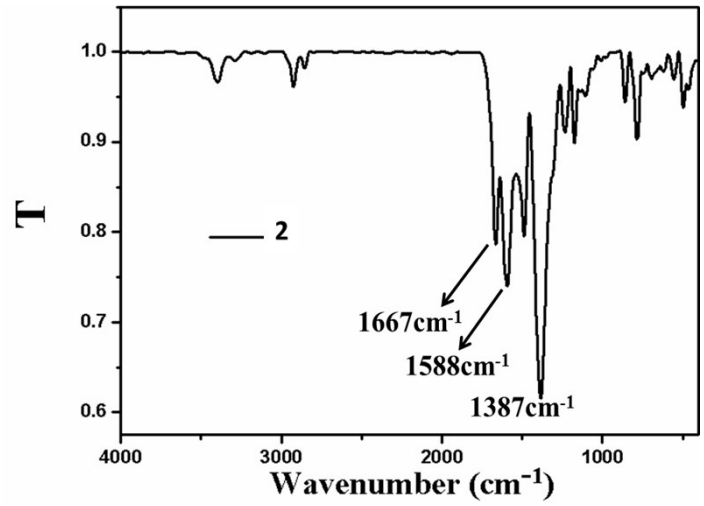

Fig.S5 IR spectrum of **2** at room temperature.

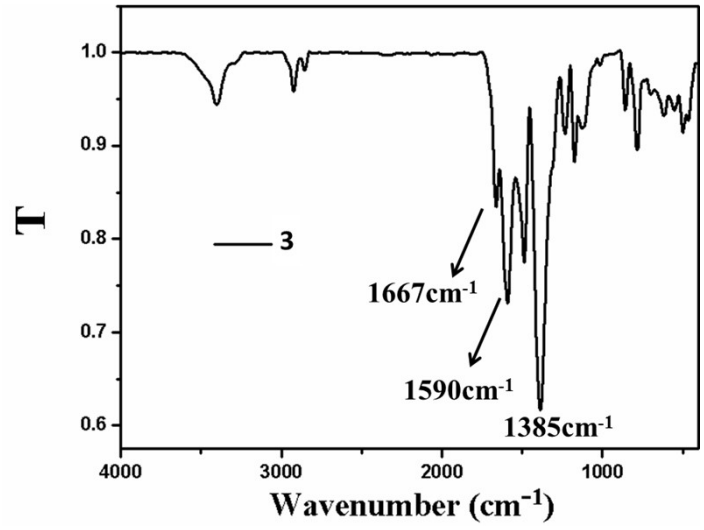

Fig.S6 IR spectrum of **3** at room temperature.

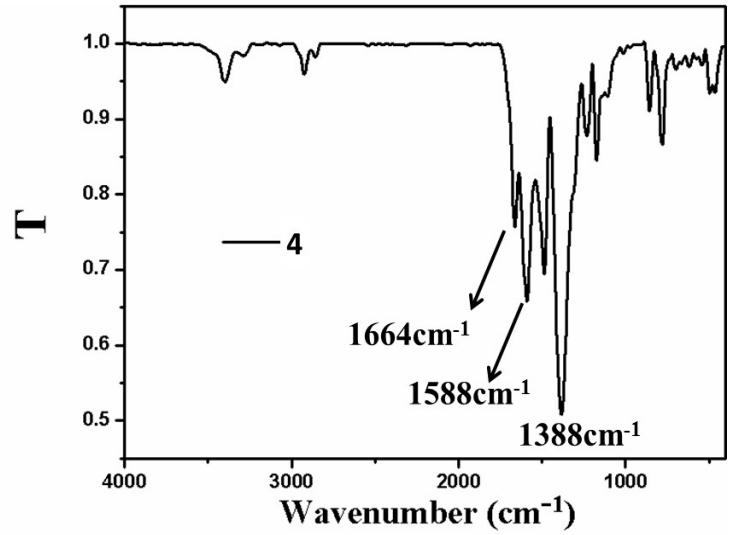

Fig.S7 IR spectrum of **4** at room temperature.

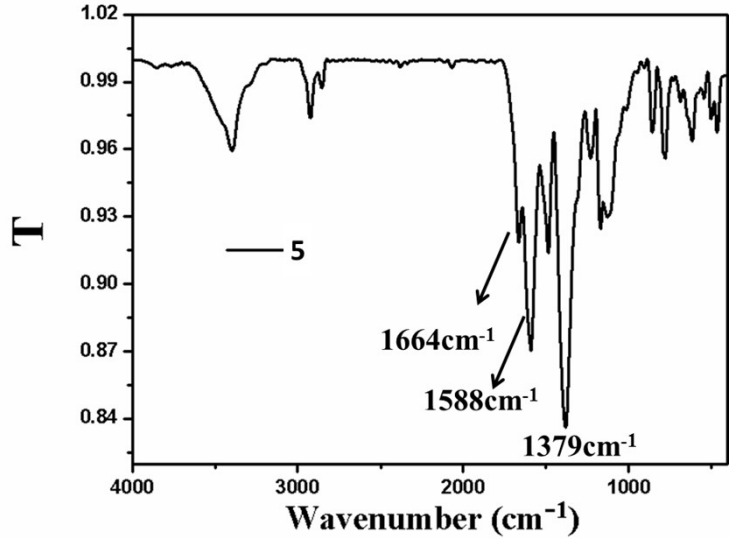

Fig.S8 IR spectrum of **5** at room temperature.

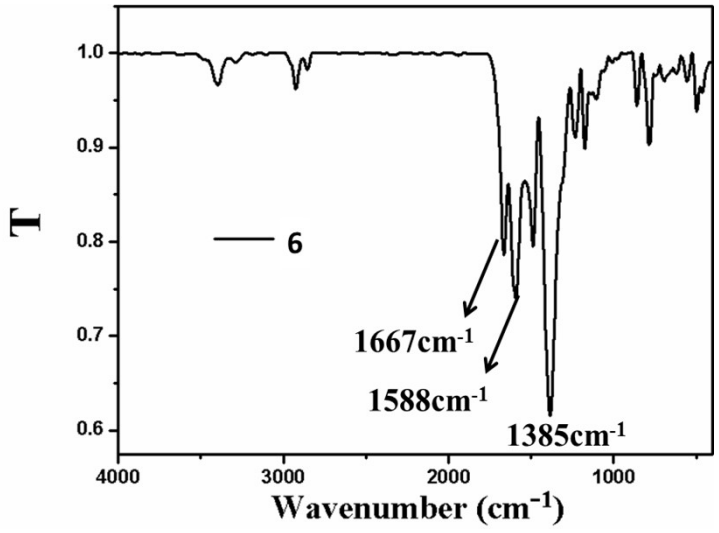

Fig.S9 IR spectrum of **6** at room temperature.

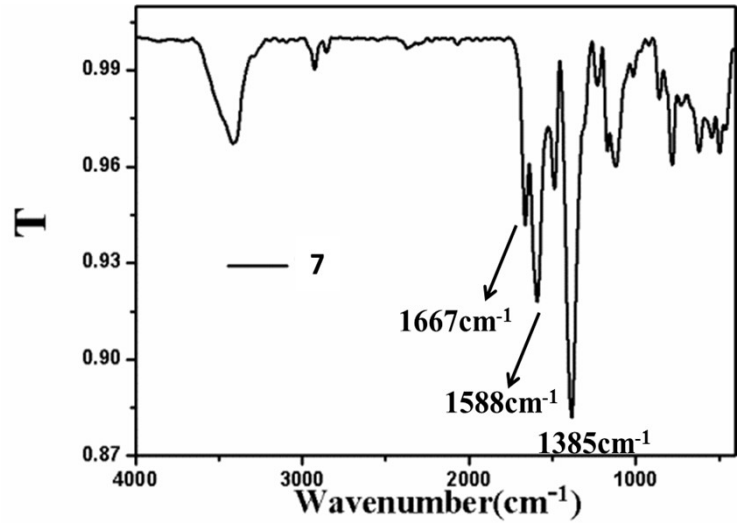

Fig.S10 IR spectrum of **7** at room temperature.

Table S1. Detailed attributes of the IR data for 1-7.

	1	2	3	4	5	6	7
ν_{O-H}	3404	3394	3411	3404	3396	3394	3411
ν_{-CH2-}	2928,2860	2928,2853	2926,2856	2928,2860	2928,2853	2928,2856	2926,2863
ν_{asCOO^-}	1665,1590	1662,1588	1667,1590	1664,1588	1664,1588	1667,1596	1667,1588
$\nu_{(C=N,C=C)}$	1489	1489	1490	1489	1489	1488	1490
ν_{sCOO^-}	1388	1387	1385	1388	1379	1385	1385
$\nu_{C-N(triazine)}$	1238	1238	1236	1238	1238	1236	1236
ν_{C-N}	1171	1170	1175	1170	1179	1173	1167
ν_{Ar-H}	853,784	862,786	862,783	862,777	862,786	862,782	869,783

UV-Vis spectra of 1-7(Fig.S11-S17).

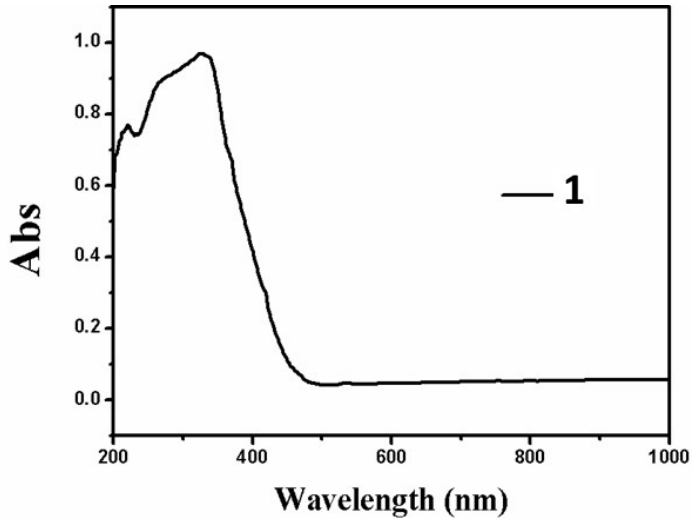

Fig.S11 Solid UV-Vis spectrum of **1** at room temperature.

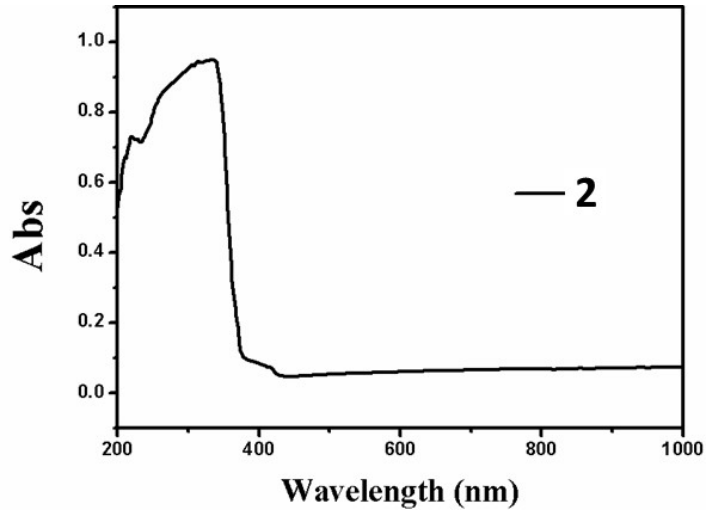

Fig.S12 Solid UV-Vis spectrum of **2** at room temperature.

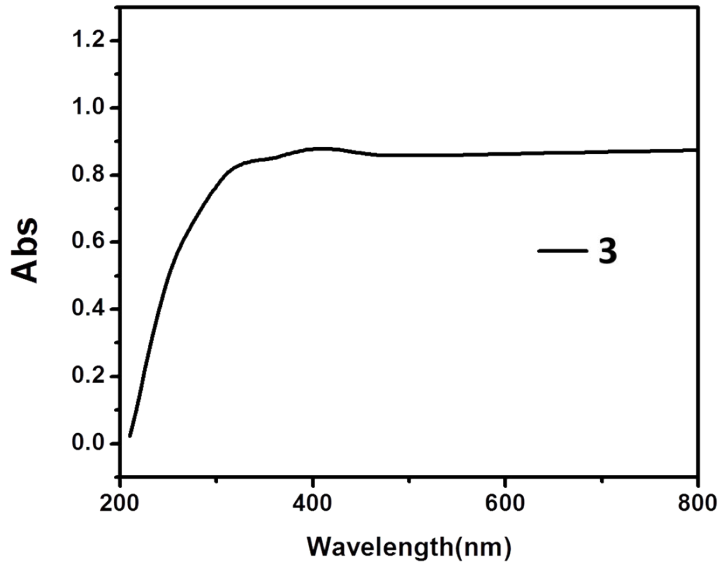

Fig.S13 Solid UV-Vis spectrum of **3** at room temperature.

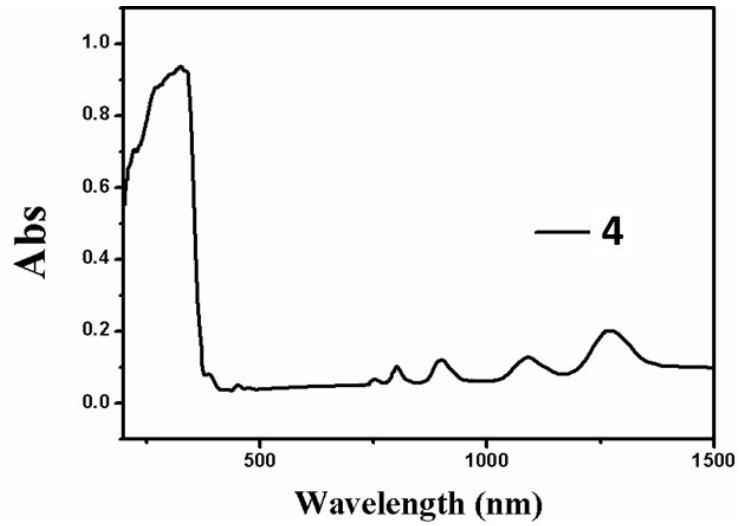

Fig.S14 Solid UV-Vis spectrum of **4** at room temperature.

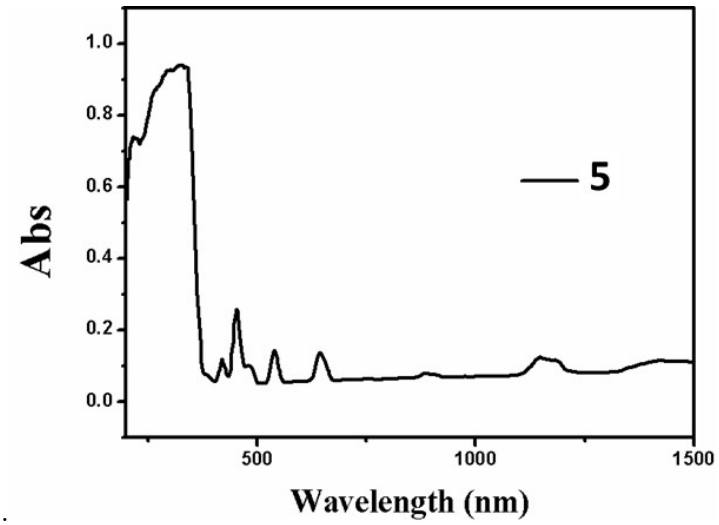

Fig.S15 Solid UV-Vis spectrum of **5** at room temperature.

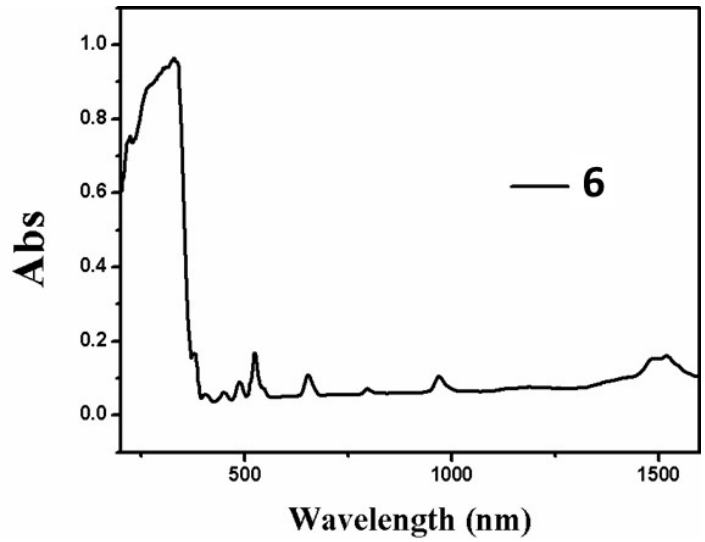

Fig.S16 Solid UV-Vis spectrum of **6** at room temperature.

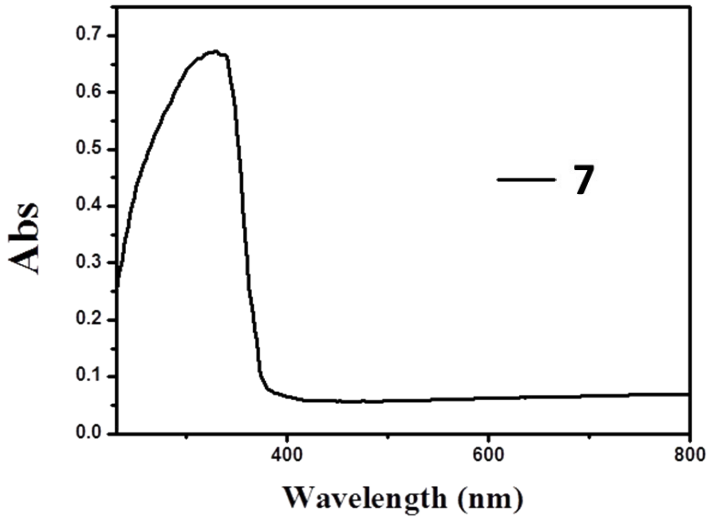

Fig.S17 Solid UV-Vis spectrum of **7** at room temperature.

Table S2. Detailed attributes of UV-Vis data for 1-7.[1-3]

Compound	Peak of adsorption/(nm)	Attributes
1	221, 226, 326	□π→π*
2	219, 265, 331	□π→π*
3	245, 327	π→π*
	1270, 1091,901	$^6H_{15/2}\rightarrow{}^6F_J$
	801,753	(J=11/2,9/2,7/2,5/2,3/2)
4	475, 451	$^6H_{15/2}\rightarrow{}^4F_J$ (J=9/2, 15/2)

	221, 268, 324	π→π*
	1146, 886	$^5I_8 \rightarrow {}^5I_6$ (J=6, 5)
	644, 539, 480	$^5I_8 \rightarrow {}^5F_J$ (J=5, 4, 3)
	454, 421, 384	$^5I_8 \rightarrow {}^5G_J$ (J=6, 5, 3)
5	218, 264, 324	π→π*
	1479, 1521	$^4I_{15/2} \rightarrow {}^4I_{1/2}$
	970, 798	$^4I_{15/2} \rightarrow {}^4I_J$ (11/2, 9/2)
	653, 486	$^4I_{15/2} \rightarrow {}^4I_F$ (9/2, 7/2)
6	221, 265, 327	□π→π*
7	251, 330	□π→π*

TG curves of 1-7(Fig.S18-S24).

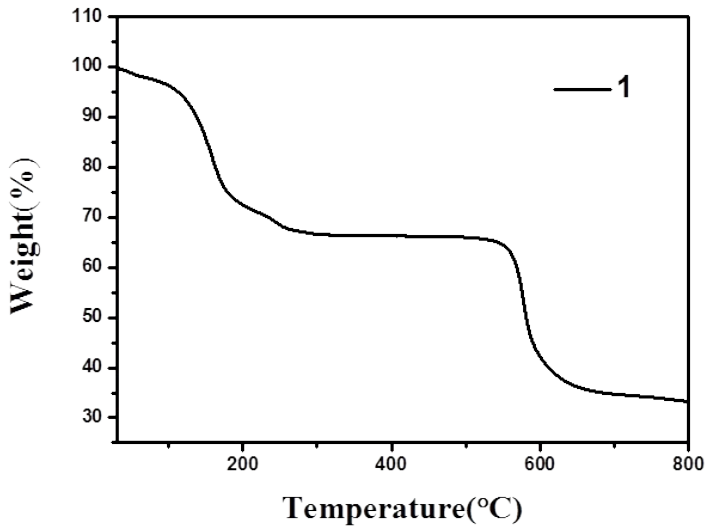

Fig.S18 TG curve of **1**.

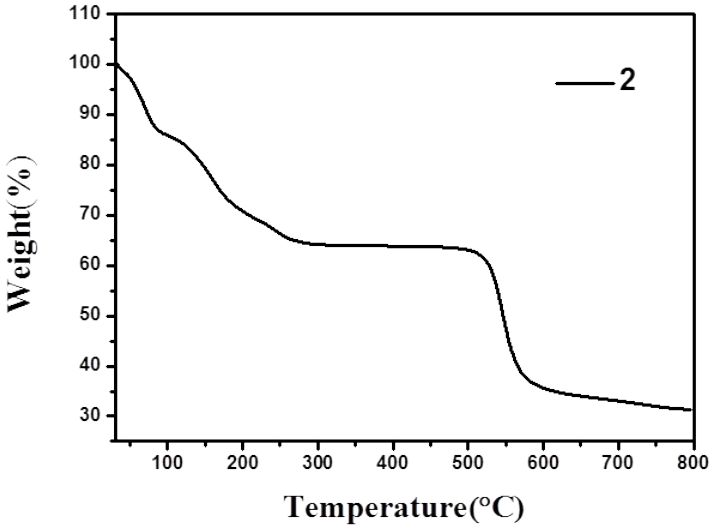

Fig.S19 TG curve of **2**.

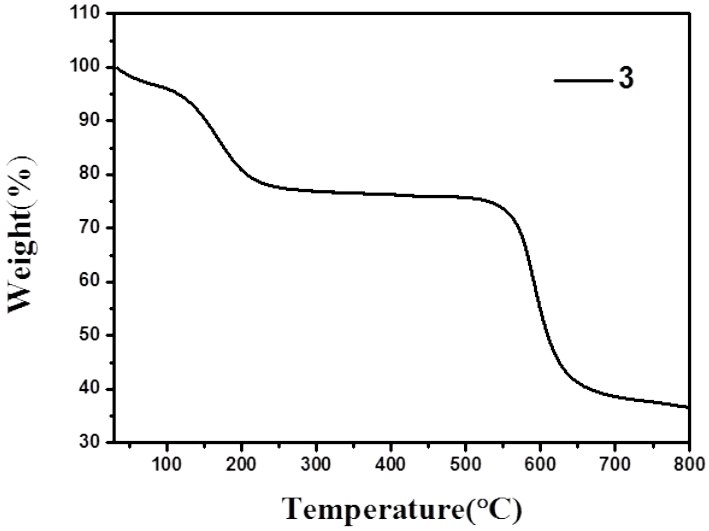

Fig.S20 TG curve of **3**.

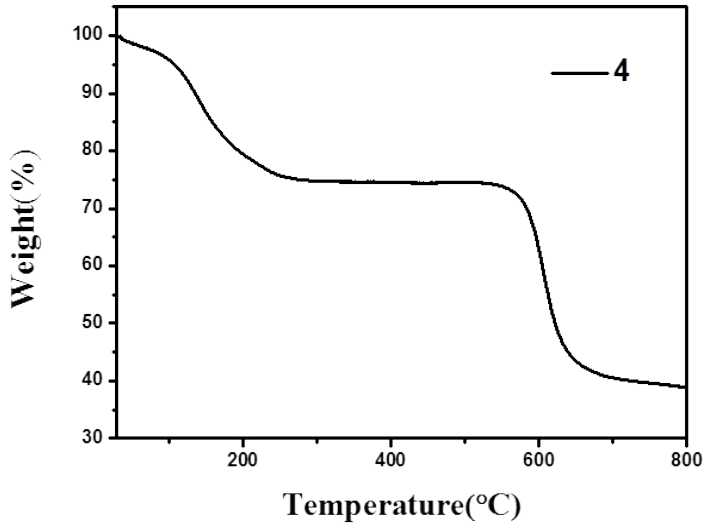

Fig.S21 TG curve of **4**.

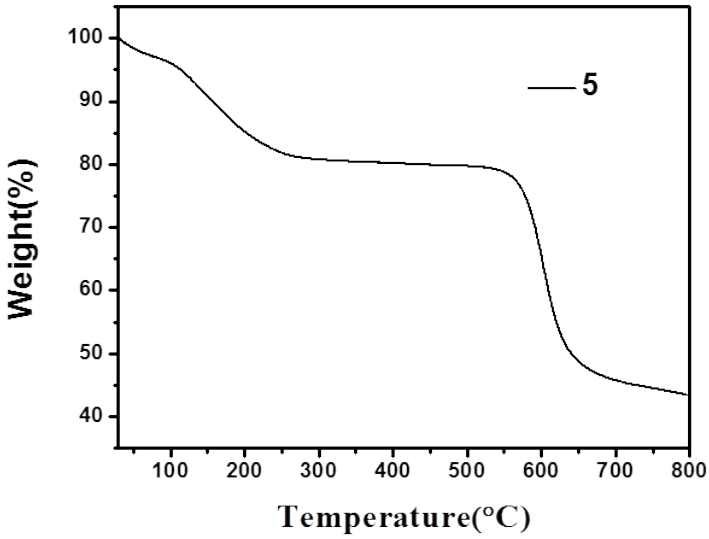

Fig.S22 TG curve of **5**.

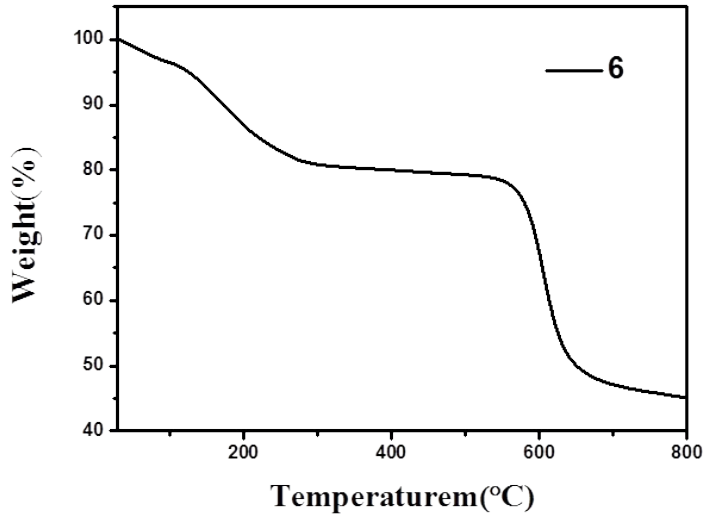

Fig.S23 TG curve of **6**.

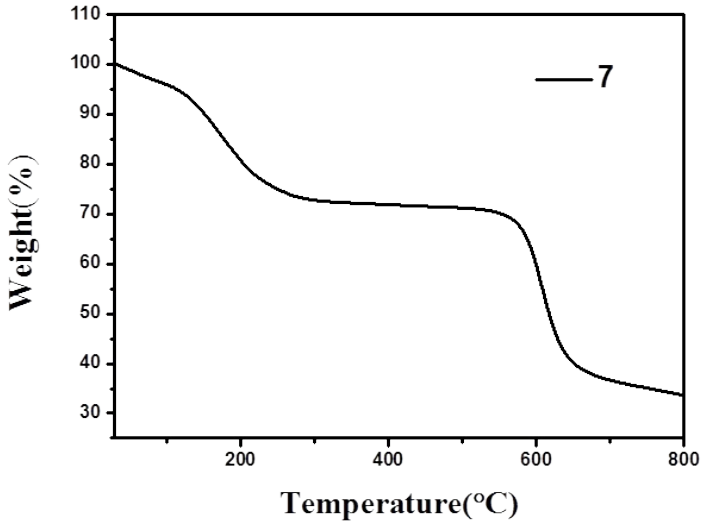

Fig.S24 TG curve of **7**.

Solid fluorescence spectra of 3 and 4.

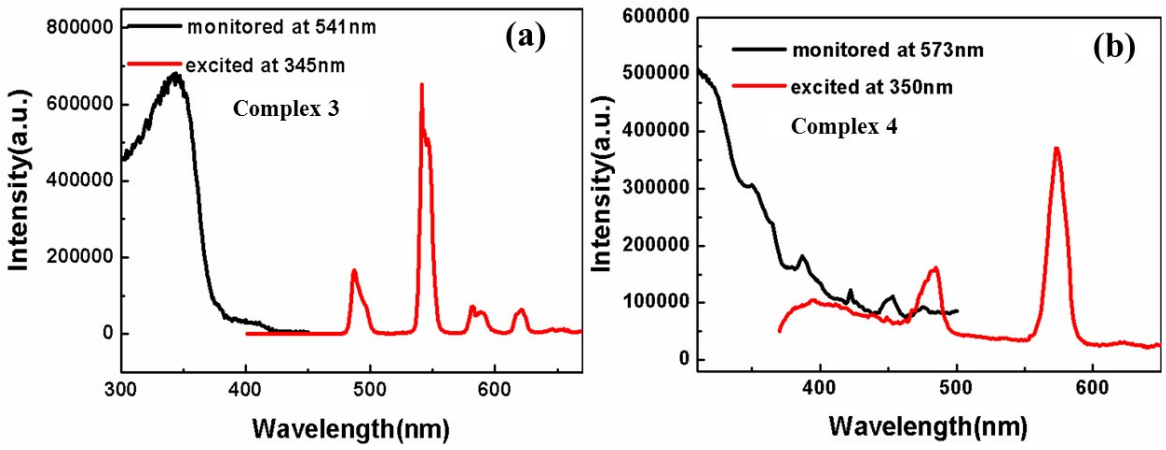

Fig.S25 Solid excitation and emission spectra of **3** and **4** show in (a) and (b).

The stability test of 1 soaked in H_2O and cyclohexane for 12h.

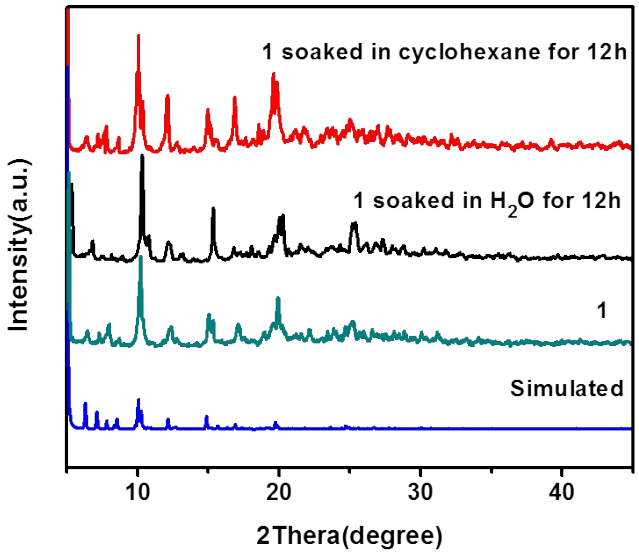

Fig.S26 The PXRD patterns of **1** soaked in H_2O and cyclohexane for 12 h.

PXRD patterns for 1 after capturing MB.

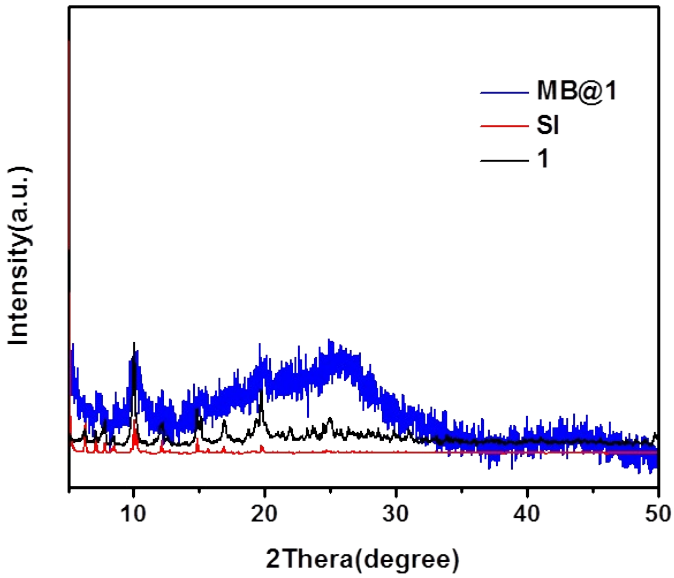

Fig.S27 PXRD patterns of **1** after capturing MB compared to simulated.

PXRD patterns for 1 after capturing I_2 and releasing I_2.

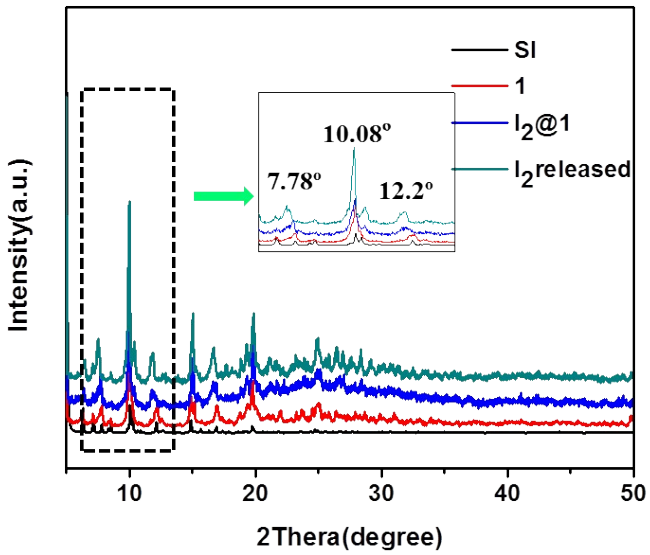

Fig. S28. PXRD patterns of I_2@**1** and I_2 released compared with simulated. The insert picture represents the angular movement of the peak at 7.78, 10.08 and 12.2 degrees.

IR and UV-vis spectra for 1 after capturing I_2.

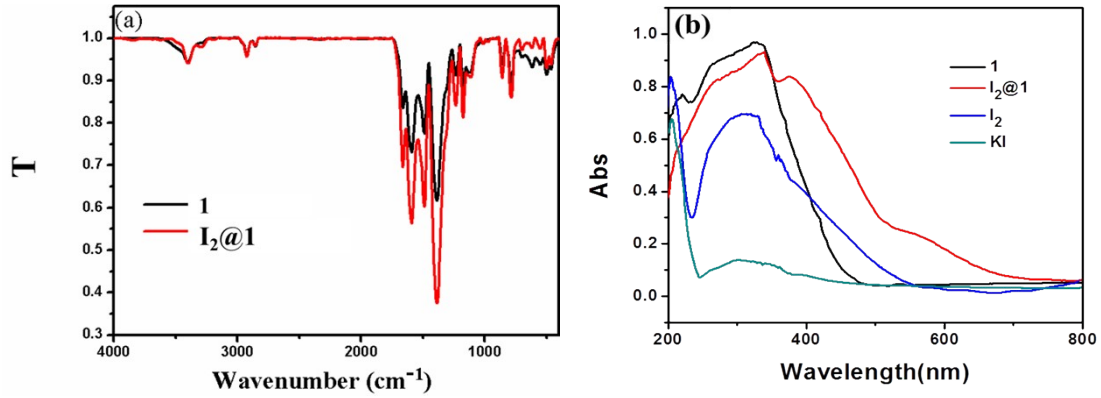

Fig. S29. (a) IR spectra of **1** and I_2@**1**. (b) Solid-state UV-Vis spectra of **1**, I_2@**1**, I_2 and KI.

PXRD Pawley refinement of I_2@1.

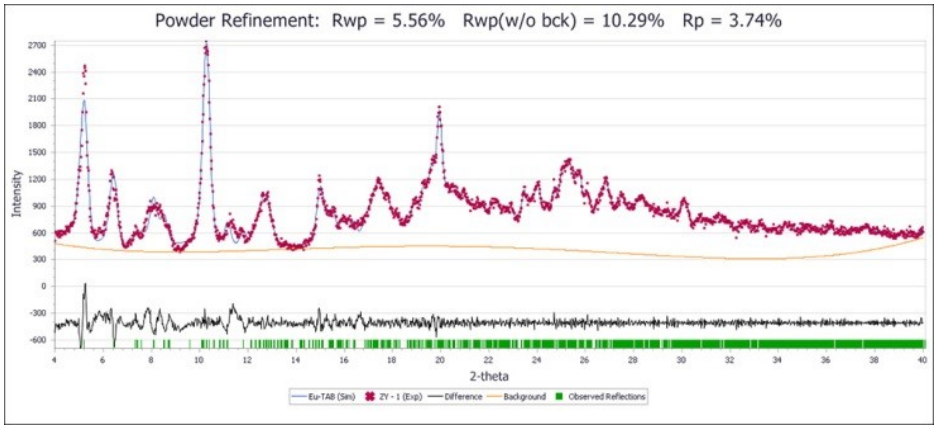

Fig.S30. PXRD Pawley refinement of I_2@**1** (Lattice Type: monoclinic, space group: $P2_1/C$ (14). Rwp = 5.56%, Rp=3.74%, a = 28.869(7) Å, b = 22.218(6) Å, c = 15.166(4) Å, alpha = 90.0000, beta = 103.4689, gamma = 90.0000, λ = 1.540562 Å, GOF=1.038). Experimental data are shown as blue plots, the refined profiles as the purple petal-shaped points, and the difference under them as green plots. Reflection positions are marked with black. The detailed refinement data are listed in Table S7.

The cycle tests of adsorption-desorption of I_2 with 1.

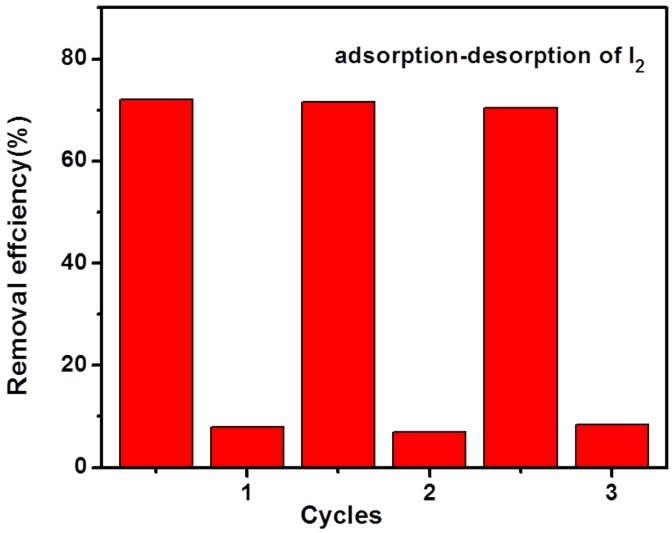

Fig.S31. The cycle tests of adsorption-desorption of I_2 with **1**.

The first-order-equation fitting model of adsorption to I_2 with 1.

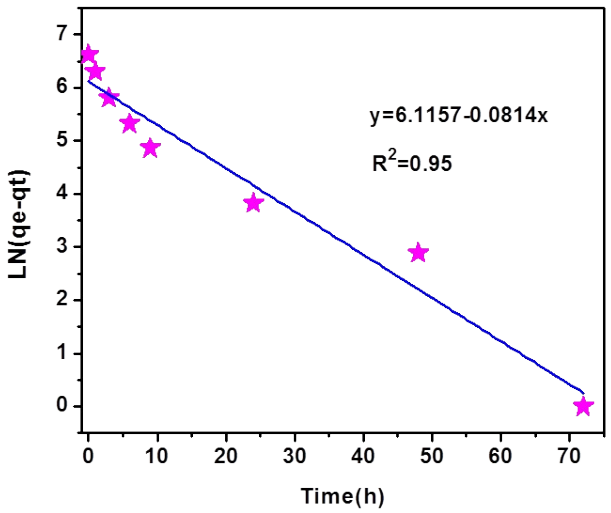

Fig.S32. The adsorption of iodine with **1** fitted with first-order-equation kinetic model. The constant R^2 is 0.95 which is lower than the constant R^2 0.99 fitted by pseudo-second-order.

Table S3. Crystallographic data of 1-3*.

Complexes	**1**	**2**	**3**
Molecular formula	$C_{48}H_{30}N_{12}O_{12}Eu_2$	$C_{48}H_{30}N_{12}O_{12}Gd_2$	$C_{48}H_{30}N_{12}O_{12}Tb_2$
Formula weight (g/mol)	1270.78	1281.34	1284.68
Crystal system	Monoclinic	Monoclinic	Monoclinic
Space group	$P2_1/c$	$P2_1/c$	$P2_1/c$
a (Å)	28.869(7)	28.7882(13)	29.106(5)
b (Å)	22.218(6)	22.6249(11)	21.998(4)
c (Å)	15.166(4)	15.2517(7)	15.091(3)
α (°)	90	90	90
β (°)	103.467(4)	103.626(10)	103.308(3)
γ (°)	90	90	90
V (Å^3)	9460(4)	9654.3(8)	9403(3)
Z	4	4	4
D g/cm-3	0.892	0.882	0.908
F(000)	2496	2504	2512
μ(Mo-Kα)/mm^{-1}	1.353	1.400	1.531
θ (°)	0.73-29.33	1.16-29.97	1.17-31.42
Reflections collected	56217	56217	56217
Parameters	667	667	668
Δ(ρ) (e Å^{-3})	7.202 and -4.552	1.233 and -1.133	8.301 and -6.798
Goodnessof fit on F^2	1.038	1.030	1.019
Final R indices[$I>2\sigma(I)$]	R_1=0.0446 wR_2=0.1127	R_1=0.0444 wR_2=0.1119	R_1=0.0440 wR_2=0.1107
Final R indices[all data]	R_1=0.0570 wR_2=0.1154	R_1=0.0569 wR_2=0.1146	R_1=0.0564 wR_2=0.1134

*$R = \Sigma||F_O| - |F_c||/\Sigma|F_O|$, $wR_2 = [\Sigma w(F_O^2 - F_c^2)^2/\Sigma w(F_O^2)^2]^{1/2}$, $[F_O>\sigma(F_O)]$

Table S4. Crystallographic data of 4-7*.

Complexes	**4**	**5**	**6**	**7**
Molecular formula	$C_{48}H_{30}N_{12}O_{12}Dy_2$	$C_{48}H_{30}N_{12}O_{12}Ho_2$	$C_{48}H_{30}N_{12}O_{12}Er_2$	$C_{48}H_{30}N_{12}O_{12}Y_2$
Formula weight (g/mol)	1291.84	1296.70	1301.36	1144.66
Crystal system	Monoclinic	Monoclinic	Monoclinic	Monoclinic
Space group	$P2_1/c$	$P2_1/c$	$P2_1/c$	$P2_1/c$
a (Å)	29.1041(11)	29.062(2)	28.9870(14)	29.082(8)
b (Å)	21.9828(8)	22.0255(15)	22.1223(11)	21.972(6)
c (Å)	15.0854(5)	15.0555(10)	15.01309(8)	15.182(4)
α (°)	90	90	90	90
β (°)	103.184(2)	103.2030(10)	103.227(2)	103.381(16)
γ (°)	90	90	90	90
V (Å^3)	9397.1(6)	9382.2(11)	9445.4(8)	9438.0(4)
Z	4	4	4	4
D g/cm-3	0.913	0.918	0.915	0.806
F(000)	2520	2528	2536	2304
μ(Mo-Kα)/mm^{-1}	1.617	1.714	1.804	1.263
θ (°)	1.94-27.09	0.72-27.18	1.7 to 29.32	1.93 to 28.68
Reflections collected	56217	56217	56217	125315
Parameters	667	668	668	667
Δ(ρ) (e Å^{-3})	6.528 and -4.461	5.000 and -3.28	8.634 and -6.944	4.027 and -2.192
Goodnessof fit on F^2	1.018	1.020	1.030	0.931
Final R indices[I>2σ(I)]	R_1=0.0441 wR_2=0.1107	R_1=0.0442 wR_2=0.1109	R_1=0.0448 wR_2=0.1121	R_1=0.0970 wR_2=0.2365
Final R indices[all data]	R_1=0.0564 wR_2=0.1133	R_1=0.0566 wR_2=0.1135	R_1=0.0571 wR_2=0.1146	R_1=0.1564 wR_2=0.2573

*$R = \Sigma||F_O| - |Fc||/\Sigma|F_O|$, $wR_2 = [\Sigma w(F_O^2 - F_c^2)^2/\Sigma w(F_O^2)_2]^{1/2}$, $[F_O>4\sigma(F_O)]$

Table S5. Selected distances (Å) for 1-7.

1					
Eu(1)-O(1)	2.298(3)	Eu(1)-O(10)	2.356(3)	Eu(2)-O(5)	2.607(4)
Eu(1)-O(5)	2.356(3)	Eu(1)-O(11)	2.389(3)	Eu(2)-O(8)	2.323(3)
Eu(1)-O(6)	2.267(3)	Eu(2)-O(2)	2.234(4)	Eu(2)-O(9)	2.380(3)
Eu(1)-O(7)	2.345(3)	Eu(2)-O(3)	2.265(3)	Eu(2)-O(11)	2.547(3)
Eu(1)-O(8)	2.603(3)	Eu(2)-O(4)	2.309(4)	Eu(2)-O(12)	2.379(3)
Eu(1)-O(9)	2.567(3)				
[1] X, 3/2-Y, -1/2+Z. [2] -X, 2-Y, 2-Z.					
2					
Gd(1)-O(1)	2.314(3)	Gd(1)-O(10)	2.398(3)	Gd(2)-O(5)	2.619(4)
Gd(1)-O(5)	2.356(3)	Gd(1)-O(11)	2.412(3)	Gd(2)-O(8)[2]	2.323(3)
Gd(1)-O(6)	2.298(3)	Gd(2)-O(2)	2.259(4)	Gd(2)-O(9)[2]	2.400(3)
Gd(1)-O(7)	2.346(3)	Gd(2)-O(3)	2.291(3)	Gd(2)-O(11)	2.560(3)
Gd(1)-O(8)	2.616(3)	Gd(2)-O(4)	2.304(4)	Gd(2)-O(12)	2.421(3)
Gd(1)-O(9)	2.575(3)				
[1]X, 3/2-Y, 1/2+Z. [2] X, 3/2-Y, -1/2+Z.					
3					
Tb(1)-O(1)	2.296(3)	Tb(1)-O(10)	2.341(3)	Tb(2)-O(5)	2.600(4)
Tb(1)-O(5)	2.367(3)	Tb(1)-O(11)	2.377(3)	Tb(2)-O(8)[2]	2.332(3)
Tb(1)-O(6)	2.251(3)	Tb(2)-O(2)	2.224(4)	Tb(2)-O(9)[2]	2.370(3)
Tb(1)-O(7)	2.359(3)	Tb(2)-O(3)	2.254(3)	Tb(2)-O(11)	2.542(3)
Tb(1)-O(8)	2.597(3)	Tb(2)-O(4)	2.326(4)	Tb(2)-O(12)	2.358(3)
Tb(2)-O(9)	2.564(3)				
[1] X, 3/2-Y, 1/2+Z. [2] X, 3/2-Y, -1/2+Z.					
4					
Dy(1)-O(1)	2.298(3)	Dy(1)-O(10)	2.340(3)	Dy(2)-O(5)	2.602(4)
Dy(1)-O(5)	2.365(3)	Dy(1)-O(11)	2.378(3)	Dy(2)-O(8)[2]	2.336(3)
Dy(1)-O(6)	2.250(3)	Dy(2)-O(2)	2.222(4)	Dy(2)-O(9)[2]	2.368(4)
Dy(1)-O(7)	2.358(3)	Dy(2)-O(3)	2.252(3)	Dy(2)-O(11)	2.539(3)

Dy(1)-O(8)	2.596(3)	Dy(2)-O(4)	2.328(4)	Dy(2)-O(12)	2.357(3)
Dy(1)-O(9)	2.566(3)				

[1] X, 3/2-Y, 1/2+Z. [2] X, 3/2-Y, -1/2+Z.

5

Ho(1)-O(1)	2.297(3)	Ho(1)-O(10)	2.344(3)	Ho(2)-O(5)	2.597(4)
Ho(1)-O(5)	2.362(3)	Ho(1)-O(11)	2.376(3)	Ho(2)-O(8)[2]	2.331(3)
Ho(1)-O(6)	2.252(3)	Ho(2)-O(2)	2.224(4)	Ho(2)-O(9)[2]	2.366(3)
Ho(1)-O(7)	2.356(3)	Ho(2)-O(3)	2.253(3)	Ho(2)-O(11)	2.536(3)
Ho(1)-O(8)	2.592(3)	Ho(2)-O(4)	2.325(4)	Ho(2)-O(12)	2.361(3)
Ho(1)-O(9)	2.561(3)				

[1] X, 3/2-Y, 1/2+Z. [2]+X, 3/2-Y, -1/2+Z.

6

Er(1)-O(1)	2.302(3)	Er(1)-O(10)	2.353(3)	Er(2)-O(5)	2.609(4)
Er(1)-O(5)	2.361(3)	Er(1)-O(11)	2.389(3)	Er(2)-O(8) [2]	2.334(3)
Er(1)-O(6)	2.259(3)	Er(2)-O(2)	2.229(4)	Er(2)-O(9)[2]	2.375(4)
Er(1)-O(7)	2.353(3)	Er(2)-O(3)	2.259(3)	Er(2)-O(11)	2.540(3)
Er(1)-O(8)	2.601(3)	Er(2)-O(4)	2.321(4)	Er(2)-O(12)	2.372(3)
Er(1)-O(9)	2.567(3)				

[1]X, 3/2-Y, 1/2+Z. [2] X, 3/2-Y, -1/2+Z.

7

Y(1)-O(1)	2.652(5)	Y(1)-O(9)[1]	2.363(4)	Y(2)-O(8)[2]	2.337(4)
Y(1)-O(2)	2.561(4)	Y(1)-O(11)[1]	2.323(4)	Y(2)-O(9)[2]	2.570(4)
Y(1)-O(3)	2.309(4)	Y(2)-O(1)	2.354(4)	Y(2)-O(10)	2.369(4)
Y(1)-O(4)	2.342(4)	Y(2)-O(2)	2.368(4)	Y(2)-O(11)	2.610(4)
Y(1)-O(5)	2.248(4)	Y(2)-O(7)	2.300(4)	Y(2)-O(12)	2.248(4)
Y(2)-O(6)	2.224(5)				

[1] X, 1/2-Y, 1/2+Z. [2]1-X, 1/2+Y, 1/2-Z.

Table S6. The comparison of I_2 adsorption amount in recent years.

Compound	the adsorption amount	Temperature(K)	Refs.

	of iodine($mg \cdot g^{-1}$)		
Ca-MOF	460	RT*	Chemistry- A European Journal, 2018.[4]
	250	348	
HKUST-1 @polymer	720	RT*	Advanced Functional Materials, 2018.[5]
Cu-MOF	492.37	RT*	Chinese Journal of Inorganic Chemistry, 2015.[6]
Cu-MOF	144	RT*	Journal of Radioanalytical and Nuclear Chemistry, 2020.[7]
1	758.72	RT*	This work

*RT=room temperature. HKUST=Hong Kong University of Science and Technology

Table S7. Reflex summary report for Pawley refinement of I_2@1.

Reflex Summary Report for Pawley Refinement of I_2@**1**			
Final R_{wp}	5.56%	Final R_p	3.74%
Final R_{wp}(without background)	10.29%	Final CMACS	0.03%
	Lattice Parameter	Value	
Lattice Type: Monoclinic, Space Group: $P\ 2_1/_C$ (14)	a	28.86688 ± 0.00311	
	b	22.21632 ± 0.00269	
	c	15.16582 ± 0.00162	
	α	90	
	β	103.47024 ± 0.00562	
	γ	90	

References

1 N. Zhang, Y.-H. Xing and F.-Y. Bai, A Uranyl-Organic Framework Featuring Two-Dimensional Graphene-like Layered Topology for Efficient Iodine and Dyes Capture, *Inorganic Chemistry*, 2019, **58**, 6866-6876.

2 X.-L. Qu and B. Yan, Stable Tb(III)-Based Metal–Organic Framework: Structure, Photoluminescence, and Chemical Sensing of 2-Thiazolidinethione-4-carboxylic Acid as a Biomarker of CS2, *Inorganic Chemistry*, 2018, **58**, 524-534.

3 Y. Wang, S.-H. Xing, F.-Y. Bai, Y.-H. Xing and L.-X. Sun, Stable Lanthanide–Organic Framework Materials Constructed by a Triazolyl Carboxylate Ligand: Multifunction Detection and White Luminescence Tuning, *Inorganic Chemistry*, 2018, **57**, 12850-12859.

4 A. Gładysiak, T. N. Nguyen, M. Spodaryk, J. H. Lee, J. B. Neaton, A. Züttel and K. C. Stylianou, Incarceration of Iodine in a Pyrene‐Based Metal‐Organic Framework, *Chemistry- A European Journal*, 2018, DOI: 10.1002/chem.201805073.

5 B. Valizadeh, T. N. Nguyen, B. Smit and K. C. Stylianou, Porous Metal-Organic Framework@Polymer Beads for Iodine Capture and Recovery Using a Gas-Sparged Column, *Advanced Functional Materials*, 2018, **28**, 1-6.

6 H. C. L. Z. Y. M. F. J. J.-J. B. Jun-Feng, A M icroporous 3D MOF Constructed from an Acylamide Tetracid Ligand： Efective Reversible Iodine Adsorption Property, *Chinese Journal of Inorganic Chemistry*, 2015, **31**, 2103-2110.

7 M. Li, G. Yuan, Y. Zeng, Y. Yang, J. Liao, J. Yang and N. Liu, Flexible surface-supported MOF membrane via a convenient approach for efficient iodine adsorption, *Journal of Radioanalytical and Nuclear Chemistry*, 2020, **324**, 1167-1177.